공학석사 학위논문

Simple synthesis of small-sized and water well-dispersed multifunctional iron oxide nanoparticles

물에 잘 분산되는 작은 크기의 다기능 산화철 나노입자의 합성

2013년 2월

서울대학교 대학원
융합과학부 나노융합전공
양 경 모

Simple synthesis of small-sized and water well-dispersed multifunctional iron oxide nanoparticles

물에 잘 분산되는 작은 크기의 다기능 산화철 나노입자의 합성

지도교수 박 원 철
이 논문을 공학석사 학위논문으로 제출함

2013년 2월

서울대학교 대학원
융합과학부 나노융합전공
양 경 모

양경모의 석사 학위논문을 인준함
2013년 2월

위 원 장 _____ (인)
부위원장 _____ (인)
위 원 _____ (인)

Abstract

Multifunctional water well-dispersed iron oxide nanoparticles have been synthesized by a simple polyol process. In this work, non-toxic Polyethylene glycol (PEG, MW = 600) was used as both solvent and capping agent. As a result, well-dispersed iron oxide nanoparticles with high stability in aqueous solution were obtained. The sizes of the nanoparticles were controlled by varying the reaction temperature. During the synthesis, terminal hydroxyl group of PEG was partially oxidized and converted to carboxylic acid group via oxidation and acted as surfactants. To gain a better understanding of PEG layer coated on the iron oxide nanoparticles surface, we measured the as-synthesized iron oxide nanoparticles by using Fourier transform infrared spectroscopy (FT-IR) coupled with Thermogravimetric analyzer (TGA). The iron oxide nanoparticles were also characterized by using transmission electron microscopy (TEM) and dynamic light scattering (DLS). For example, iron oxide nanoparticles of 4.11 ± 0.36 nm by measuring 100 pieces of TEM image have a 3.81 nm crystal size which were matched with Debye-Scherrer equation from XRD patterns. Hydrodynamic size of 4.11 ± 0.36 nm iron oxide nanoparticles in pure water was measured to be 7.18 ± 0.89 nm by using DLS. Moreover, the water dispersion of the as-synthesized iron oxide nanoparticles were very stable over a broad pH range in the presence of salts.

Further functionalization of the as-synthesized iron oxide nanoparticles surface were conducted for investigating the possibility to multifunctional nanoparticles. The as-synthesized iron oxide nanoparticles were functionalized with amine group using general EDC / NHS coupling. Subsequently, Rhodamine b isothiocyanate (RITC) and (2-(ρ-Isothiocyanatobenzyl)-1,4,7- triazacyclononane - N,N′,N,″-triacetic acid trihydrochloride) ((ρ-SCN-Bn)-NOTA) were introduced to iron oxide nanoparticles using surface amine group reaction with isothiocyanate group of RITC, NOTA complex via thiourea bonding formation. Photoluminescence spectroscopy (PL) spectrum showed that RITC molecules were conjugated to the iron oxide nanoparticles surface. According to the results, the stably water dispersed and small-sized iron oxide nanoparticles are expected to be used for multimodal biological imaging.

keyword: Iron oxide nanoparticles, PEGylation, Polyol synthesis, Multifunctional nanoparticles

Student Number: 2011-22756

Contents

List of table, schemes, and figures

h aging time. Image taken at (a) 20,000 × magnification, (b) 40,000 × magnification, and (c) 100,000 × magnification, respectively. (d) Size distribution of iron oxide nanoparticles from randomly selected 100 pieces of TEM images.

Fig 4. TEM images of as-synthesized iron oxide nanoparticles. Image taken at (a) 20,000 × magnification, (b) 40,000 × magnification, and (c) 100,000 × magnification, respectively.

Fig 5. TEM images of the as-synthesized iron oxide nanoparticles with different aging times of (a) 0 h, (b) 0.5 h, (c) 1.5 h, and (d) 3 h, respectively. All images are taken at 40,000 × magnification.

Fig 6. DLS data of the iron oxide nanoparticles prepared using ferric acetylacetonate with different aging times of no aging (dashed line, 6.15 ± 0.61 nm from TEM observations), 0.5 h aging (dashed dot line, 8.01 ± 0.82 nm from TEM observations), 1.5 h aging (solid line, 9.99 ± 1.44 nm from TEM observations) respectively.

Fig 7. (a, b) low magnification and (c) relatively higher magnification TEM images of 4.11 ± 0.36 nm iron oxide nanoparticles prepared using ferric nitrate. (d) Size distribution of iron oxide nanoparticles from randomly selected 100 pieces of TEM images.

Fig 8. TEM images of the iron oxide nanoparticles using ferric nitrate with different heating rate of (a, b) 1K / min, and (c, d) 10 K / min. (The heating temperature for both samples is 538 K and

maintain at that temperature for 30 min).

Fig 9. TEM images of the iron oxide nanoparticles synthesized at 568 K Image taken at (a) 20,000 × magnification, (b) 40,000 × magnification, (c) 100,000 × magnification, and (d) 300,000 × magnification, respectively.

Fig 10. DLS data of the 4.11 ± 0.36 nm (from TEM observation) iron oxide nanoparticles using ferric nitrate (dashed line) and the aggregated iron oxide nanoparticles synthesized at 568 K (solid line).

Fig 11. (a) XRD patterns of the as-synthesized iron oxide nanoparticles. 4.11 ± 0.36 nm (from TEM observation) iron oxide nanoparticles were synthesized using ferric nitrate as precursors. 6.15 ± 0.61 nm, 8.01 ± 0.82 nm, 9.99 ± 1.44 nm (from TEM observation) iron oxide nanoparticles were synthesized using ferric acetylacetonate. (b) XRD patterns of (440) peak of the iron oxide nanoparticles with different diameter.

Fig 12. TGA data of the as-synthesized iron oxide nanoparticles (4.11 ± 0.36 nm from TEM observations) by using ferric nitrate

Fig 13. (a) is FT-IR spectrums of pure PEG 600 molecules. (b) FT-IR spectrum of the PEG coated iron oxide nanoparticles by using ferric acetylacetonate as precursor and, (c) by using ferric nitrate as precursor in (Fig 13 (A)). (Fig 13 (B)) show the lattice adsorption band spectrum of iron oxide nanoparticles by using ferric nitrate as precursor.

Fig 14. Gaussian fitted FT-IR spectrum of the as-synthesized iron

1. Introduction

Nanoscience is the term used to describe the research and development of materials that have at least one dimension in the nanometer size range. Nanomaterials located at between those of atoms and bulk materials in the size range that unique physical and chemical properties derived from their size and structure [1-3]. Nanomaterials have attracted much attention for biomedical applications because of their sufficiently small size combined with newly property [5]. There are already many research existed using nanomaterials for improving standards in healthcare such as biomedical imaging probe [6-8], gene delivery [9], targeted drug delivery [10-12]. In particular, the development of biomedical imaging probe by using nanoparticles is very attractive research area since the nanoprobes could be used to improve quality of clinical images [13-15]. Especially, nanoparticles have attracted attention with possibilities combination of structural imaging and functional imaging techniques have important meaning [15] since the anatomical features and molecular imaging by functional imaging techniques like CT / PET have a low spatial resolution but high sensitivity, while structural imaging techniques like MR / X-ray have a high spatial resolution with low sensitivity. Especially, the use of magnetic iron oxide nanoparticles has received considerable attention in the development of multifunctional imaging probe. Since magnetic iron oxide

nanoparticles can be used as MR contrast agents naturally, through the production of spin-spin relaxation effects inducing T1 and T2 relaxation times changes [16].

1.1 Magnetic phenomena of magnetic iron oxide nanoparticles.

There are two types of most common magnetic iron oxide at room temperature, which are magnetite (Fe_3O_4) and maghemite (Υ-Fe_2O_3). Both of these materials in bulk forms exhibit ferrimagnetic behavior at room temperature due to their opposite magnetic momentum difference. More specifically, magnetite has cubic inverse spinel structure $A^{2+}B_2^{3+}O_4$. half of Fe^{3+} cations occupying the tetrahedral sites while half of Fe^{3+} cations occupying the octahedral sites along with Fe^{2+} cations when oxygen forming an fcc closed packing. The maghemite is the result of magnetite's topotactic oxidation. The net ferrimagnetism of iron oxide occurred by the Fe^{2+} in the octahedral sub-lattice by cancelling out of the antiparallel Fe^{3+} spins on tetrahedral sites and octahedral sites [17]. These ferrimagnetism of the iron oxide become superparamagnetism when their sizes were reduced below critical sizes [18] (below 20nm at room temperature in the case of iron oxide) [19]. In a bulk state ferrimagnetic iron oxide are composed of magnetic domains [20]. While size of the iron oxide becomes small enough, the number of domains decreases until there

is an only single domain. If an external magnetic field, H is applied to a magnetic iron oxide, the magnetization of materials increased with the magnetic field increased until a certain value of saturation magnetization, M_s is reached. If the external magnetic field removed, there are remnant magnetization, M_R in ferrimagnetic iron oxide nanoparticles while superparmagnetic iron oxide nanoparticles have no remnant magnetization at R.T. Since thermal energy k_BT comparable with energy barriers. Leads to a orientation of the magnetic spin randomly, as a result M_R will be zero from the Néel relaxation theory $\tau=\tau_0 \cdot \exp(KV / k_BT)$ where τ is the Néel relaxation time, τ_0 is the characteristic time, K is the anisotropy energy and V the volume of the particles and k_B is the boltzmann constant, T is the temperature.

This superparamagnetic property is quite important for biomedical imaging applications since application to the biomedical imaging, magnetic nanoparticles need to have no remnant magnetization at room temperature. Remnant magnetization could lead to agglomeration of iron oxide nanoparticles, and agglomeration in the body must be avoided to prevent blockage of blood vessels. Futhermore, magnetic nanoparticles can produce spin - spin relaxation effects due to the induced local field I. Hence, superparamagnetic iron oxide nanoparticles, which have dimensions smaller than 20 nm, are suitable to be used as MR imaging agents.

1.2 Synthetic strategy and stabilization of iron oxide nanoparticles.

The materials for biomedical applications must fulfill several things including good stability, biocompatibility, and preventing the non-specific interaction with a cell [23,24]. There are many synthetic approaches existed to produce biomedical applicable iron oxide nanoparticles. Most of the synthetic approaches can be mainly divided into two category, in wet chemical approaches, hydrolytic and non-hydrolytic [19]. First approach is hydrolytic method which takes place in aqueous solution. In hydrolytic approaches, co-precipitation method is the most important and widely used method [25]. Although the co-precipitation method is a very classical approach. It can be found early reports. In 1925, *Welo et al.* reported co-precipitation synthetic route of Fe (II) / Fe (III) in alkaline solution [26]. Co-precipitation, are involved of Fe^{2+} and Fe^{3+} ion spontaneous precipitation in aqueous medium following the simple chemical equation : $Fe^{3+}(aq) + Fe^{2+}(aq) + 8OH^- \rightarrow Fe_3O_4 + 4H_2O$. The nanoparticles prepared by co-precipitation easy for surface modification due to their naturally hydroxyl surface [27]. Feridex®, as a iron oxide nanoparticles coverd by dextran, is representative of the commercialized iron oxide based MR imaging contrast agents available in market with Food and Drug Administration (FDA) approval. The classification of commercialized iron oxide based MR imaging contrast agents are organized in (Table 1). They are commonly not uniform

with irregular morphology and broad size distribution [28]. To overcome these problems, many research group have tried to develope other synthetic methods, such as microemulsion process [29], aqueous and non aqueous sol-gel process [30-33], hydrothermal process [34].

Thermal decomposition method that are containing thermal decomposition of organometallic precursors such as ferric acetylacetonate [35] or iron oleate [36] and subsequently growth of nanoparticles in hot organic solvent with surfactant. Thermal decomposition method has several advantages, the produced iron oxide nanoparticles show regular shape, high uniformity, and high crystallinity. For example, Sun group demonstrated that decomposition of ferric acetylacetonate in the presence of phenyl ether with 1.2-hexadecandiol, oleic acid, and oleylamine [35]. By a similar method, *Park et al.* reported the preparation of monodispersed metal oxide nanoparticles by decomposition of metal oleate in the presence of oleic acid [36] Nowadays, thermal decomposition of organometalic precursor is a reliable general route to synthesize monodisperse iron oxide nanoparticles [37]. However, they need time consuming complex ligand exchange process to modifying the surface of the iron oxide nanoparticles for biomedical applications. There are many attempts to attach biocompatible hydrophilic molecules to these iron oxide nanoparticles [38-41]. Generally, ligand exchange process leads to undesired hydrodynamic size increase with limited long-term stability [42]. As surface molecules for biomedical

applications, low-molecular weight PEG have attracted a lot of attention as surface molecules from their biocompatibility. In particular, the process of covalent attachment of PEG chains to drugs, nanoparticle surface or cell is called PEGylation [43]. PEG on the surface leads to reduce nonspecific binding with a cell and improve viability and solubility by retaining a large degree of trans, gauche, trans sequence and helical conformation of the crystalline state in water. From this manner, steric stabilization of PEG molecules provides brush-like barrier in the water [44]. Hence, there are already several research papers about PEGylation of the iron oxide nanoparticles tried to attach onto the iron oxide nanoparticles [45,46] by using phosphate PEG [42] or multidentate based PEG [47]. But synthetic yield of functionalized PEG is low which makes a high price of the functionalized. For this reason, one-pot synthesis of water dispersible monodisperse iron oxide nanoparticle synthesis is important for real biomedical application. Nowadays, the synthesis of iron oxide nanoparticles in polyol medium has attracted much attention from their possibility to generate monodisperse one-pot water dispersible iron oxide nanoparticles [48]. In this study, iron oxide nanoparticles were synthesized with two types of precursor used in the presence of PEG 600 molecules. Ferric acetylacetonate was used as organometallic precursor and ferric nitrate was used as metal salt precursor. During the

synthesize, PEG molecules were partially oxidized and absorbed to the iron oxide nanoparticle surface, which was confirmed by using FT-IR. The morphology of the iron oxide nanoparticles was studied by using TEM. DLS measurements show that the particles are stably dispersed in water. Furthermore, we try to develope multifunctional iron oxide nanoparticles using as-synthesized PEGylated iron oxide nanoparticles in this study. The as-synthesized water dispersible iron oxide nanoparticles were amine functionalized using EDC / NHS coupling. Subsequently, RITC and NOTA were attached to the surface of these iron oxide nanoparticles.

Generic/ Trade name	**Ferumoxsil** *Gastromark* *Lumirem* *Abdoscan*	**Ferumoxide** *Feridex* *Resovist* *Endorem*	**Ferumoxtran** *Sinerem* *Combidex* *Clariscan*
Material/coating	Iron oxide crystals (4 - 6 nm) coated with thinner layer of dextran	Iron oxide crystals (5 - 6 nm) coated with dextran / carboxy dextran	Iron oxide crystals (10 - 50 nm) in insoluble matrix such as starch, polystyrene
Size	20 ~ 40 nm	60 ~ 150 nm	300 nm ~ 5 μm

Table 1. Classification of commercialized iron oxide nanoparticles.

Classification	Synthetic method	Aspect
Microemulsion	(1) Defined as a thermodynamically stable isotropicdispersion of two immiscible liquids by using surfactant such as AOT [51], Igepal CO-520 [52], Triton X-100 [53], Brij-97 [54]. (2)Micro domain is formed, microdomain produced by surfactant limiting the growth of particles.	Control of the particle size with the amount of surfactant. They have problem with scaling-up and residual large number of surfactant effect to the properties of particles.
Hydrothermal	(1) Hydrothermal methods conduct in a sealed container to produce high temperature aqueous solution. (2) To hydrolyze and dehydrate metal salt, pressures are elevated along with temperatures elevated. As a result, the very low solubility of the resulting metal oxides in water at these conditions to generates supersaturation [55,56].	High supersaturation can be achieved, from the low solubility of metal hydroxide and metal oxide so that fine crystals are obtained.
Sol-gel process	Divided into two process, aqueous sol-gel process and non-aqueous sol-gel process. (1) In the aqueous sol-gel process, precursor in the aqueous solution is hydrolyzed induced by water , consequently condensation occurred to form metal oxide nanoparticles [57,58], (2) In the non-aqueous sol-gel process, precursor in the organic solvent turn to metal oxide nanoparticles, through various pathways such as alkyl halide elimination [59], ether elimination [60], condensation of carboxylate group [61], C-C coupling of benzylic alchols and alkoxide molecules [62], aldd/ketimine condensation [63].	The procedure based on the hydrolysis of precursor and condensation. The particle size controllable depends on the solution composition, pH, and temperature.
Co-precipitation	(1) Most common method to prepare iron oxide nanoparticles, stioichiometric mixtures of ferric and ferrous ions are coprecipitated in aqueous media (base or a mild oxidant). (2) Particle size can be controlled by adjusting the pH and ionic strength [31, 32]	The most widely used simple synthetic method to preparation of metal oxide nanoparticles.
Thermal decomposition	(1) Decomposition of organometallic precursors such as iron cupferronates [36], ferric acetylacetonate [37], iron carboxylate [38] and iron carbonyls [64] (2) Synthesis is conducted in organic mixtures containing surfactants like oleic acid, oleylamine	The procedure based on the thermal decomposition of organometallic precursor in an hot organic solution. subsequently polymerized. It can be produce the monodisperse particles and size can be controllable in nanometer ranges.

Table 2. Preparation methods of iron oxide nanoparticles.

2. Experimental process

Chemicals.

Ferric nitrate nonahydrate, Poly ethyleneglycol MW 600 (PEG), Anhydrous sodium carbonate, Dietyl ether, Tetrahydrofuran, Sodium hydroxide and hydrochloric acid were acquired from Samchun Chemical. Ferric acetylacetonate was purchased from Strem Chemicals. Rhodamine B isothiocyanate (RITC) were purchased from Aldrich. Phosphate buffered saline (PBS, pH 7.4) and Potassium bromide (FT-IR grade, ≥99% trace metals basis) were obtained from Sigma-Aldrich. (2-(ρ-Isothiocyanatobenzyl)-1,4,7- triazacydononane -N,N′,N,″-triacetic acid trihydrochloride) ((ρ-SCN-Bn)-NOTA) was purchased from Future chem. Aqueous solutions were utilized using deionized water (DI water). All reagents were used as received.

Characterization.

X-ray diffraction (XRD) patterns of the as-synthesized iron oxide nanoparticles obtained from Rigaku Dmax 2500 diffractometer with Cu Kα radiation (λ = 1.5406 A) at 40 kV and 100 mA. Transmission electron microscopic (TEM) and high-resolution TEM (HR-TEM) images were examined on a JEOL EM-2010 microscope at accelerating voltage of 200 kV and JEM-3010 (JEOL) at accelerating voltage of 300 kV. Size and size distribution of samples were estimated by Zetasizer Nano ZS equipped with a laser operating at 633 nm He-Ne laser with back scattering detector at 173° (Malvern). Fluorescence

excitation and emission spectra were obtained by FluoroMate FS-2 (Scinco). FT-IR spectra collected with Nicolet 5700 and Nicolet 6700 using KBr pellet, (Attenuated total reflectance) ATR mode (Thermo electron corp.). Thermogravimetric analysis conducted by using TGA/DSC 1-Thermogravimetric Analyzer (Mettler-Tolledo).

2.1 Synthesis of iron oxide nanoparticles using organometallic precursor

We prepared iron oxide nanoparticles using ferric acetylacetonate as a organometallic precursor in PEG medium. To prepare 6.15 ± 0.61 nm iron oxide nanoparticles, 0.534 g (1.5 mmol) of ferric acetylacetonate mixed with 4.8 g (8 mmol) of melted PEG to get homogeneous reddish solution. The prepared solution dehydrated by heating under low preassure at 353 K in 30 min. The resulting mixture was heated to 538 K with constant heating rate 1.8 K/min. During this process, the intial reddish solution gradually changed to brownish black indicating the formation of iron oxide nanoparticles. Subsequently, the resulting solution was cooled to room temperature with heat sources removal. then washed several times with ethanol, diethyl ether mixture by centrifugation. Excess PEG and unreacted molecules were removed using ethanol. When diethyl ether was used as precipitant of iron oxide nanoparticles. All synthesis proceed under continuous nitrogen purge excluded dehydrate procedure.

2.2 Synthesis of iron oxide nanoparticles using metal salt precursor

We prepared iron oxide nanoparticles using ferric nitrate as a metal salt precursor in PEG medium. To prepare 4.11 ± 0.36 nm iron oxide nanoparticles from TEM observation, 0.404g (1 mmol) of ferric nitrate nonahydrate mixed with 12g (20 mmol) of melted PEG to get homogeneous orange colored solution. The resulting mixture was heated to 373 K with constant heating rate 10 K / min. And kept that temperature 0.5 h. Subsequently the mixture heated to 538 K in 17 min and held for 0.5 h. During this process, the intial orange colored solution gradually changed to brownish black indicating the formation of iron oxide nanoparticles. All synthesis process performed under low pressure. Subsequently, the resulting solution was cooled to room temperature then washed several times with ethanol, diethyl ether mixture by centrifugation.

2.3 Functionalization of the as-synthesized iron oxide nanoparticles

Functionalization of the as-synthesized iron oxide nanoparticles with amine group

The as-synthesized 4.11 ± 0.36 nm iron oxide nanoparticles were chosen for functionalization. To prepare amine functionalized iron oxide nanoparticles, 6g of the as-synthesized brownish-black solution

washing with ethanol, diethyl ether mixture twice by centrifugation and re-disperse in 50 ml of 0.01 M phosphate-buffered saline (PBS), pH 7.4. Then, 600 µl of EDC solution (15 mg in 1 ml 0.01M PBS, pH 7.4) and NHS (9 mg in 1 ml 0.01 M PBS, pH 7.4) solution was added and the solution stirred at R.T another 10 min. Then, 360 ul ethylenediamine was dropped into the solution. After stirring 2 hr, the amine functionalized iron oxide nanoparticles was precipitation by using centrifugation with Tetrahydrofuran (THF) as precipitant. The precipitated iron oxide nanoparticles were re-disperse in 50 ml of 0.05 M Sodium carbonated buffer (SCB), pH 9.5 to further functionalization with radioisotope chelating agents and fluorescent dye.

Conjugation of radioisotope chelating agents and fluorescent dye onto iron oxide nanoparticles.

To prepare chelating agents and fluorescent dye conjugated iron oxide nanoparticls, 500 ul of RITC (1.25 mg in 1 ml 0.05M SCB, pH 9.5) solution and 500 ul of (p-SCN-Bn)-NOTA (2.5 mg in 1 ml 0.05M SCB, pH 9.5) solution was dropped into the as-prepared solution. After stirring 6 hr, solution were mixing with THF and centrifugation. Then, precipitated products were re-disperse in DI water. The product was further purified by dialysis against DI water, using tubing with a 12,000-14,000 M_W cutoff (Zellu Trans, Roth (Germany)).

3. Result and Discussion

3.1 Synthesis of the iron oxide nanoparticles using organometallic precursor

Iron oxide nanoparticles were synthesized by using ferric acetlyacetonate as precursor with PEG 600 as a described above (Scheme 1.). PEG 600 plays a triple role as high-bioling solvent, reducing agent, and capping agents to efficiently control the particle growth and prevent aggregation in this reactions. Different sized iron oxide nanoparticles were prepared by varying the aging times. Shape and size of the as-synthesized iron oxide nanoparticles were observed by using TEM. Hydrodynamic size and size distribution were measured by using DLS. The TEM images and size distribution of the as-synthesized iron oxide nanoparticles with no aging time were shown in (Fig 1) and TEM images of the iron oxide nanoparticles with aging time of 0.5 h and 1.5 h were shown in (Fig 2, 3). DLS was used to measure the hydrodynamic size of the as-synthesized iron oxide nanoparticles in pure water. In DLS measurement, hydrodynamic size of the iron oxide nanoparticles were slightly higer from the surface molecules. Furthermore, size of the iron oxide nanoparticles was controlled with varying the aging times (Fig 4). For example, synthesis of the 6.15 ± 0.61nm from TEM observation iron oxide nanoparticles were conducted with no aging time at 538 K

while 10 nm iron oxide nanoparticles were synthesized with 1.5 h aging time, although the size distribution of the as-synthesized iron oxide nanoparticles became broadening which is matched with the DLS measurement (Fig 5, 6). The reason of the size distribution broadening of the as-synthesized iron oxide nanoparticles with the increasing aging times is well established by other researcher. To synthesize the monodisperse nanoparticles, separation of the nucleation process with the growth process is quite important [38,63]. We assumed that, during the aging procedure ferric acetylacetonate continued the decomposition, consequently continuos nucleation is occurring simultaneously with growth of the iron oxide nanoparticles. So that particle size distribution was broadening. To get more larger monodispersed iron oxide nanoparticles, higher temperatures needed for avoiding continuous nucleation during growth process. We could not obtained more monodispersed iron oxide nanoparticles. Since, PEG 600 molecule's boiling point is too low to avoiding the continuous nucleation in the aging procedure.

3.2 Synthesis of the iron oxide nanoparticles using metal salt precursor

There are early study when ferric nitrate nonahydrate powders are heated even at low temperature of 348 K for long time, ferric oxide will be obtained [65]. More recently, Xu et al reported the preparation of magnetite nanoparticles by using sol-gel reaction of ferric nitrate

in ethyleneglycol medium [66].

In this study, synthesis of the iron oxide nanoparticles conducted using ferric nitrate in the presence of the PEG 600 as described above (Scheme 2). The shape and size of the as-synthesized iron oxide nanoparticles were observed by using TEM. Hydrodynamic size and size distribution were measured by using DLS. The TEM images of as-synthesized 4.11 ± 0.36 nm iron oxide nanoparticles shown in (Fig 7). Hydrodynamic size of the as-synthesized iron oxide nanoparticles were measured 7.18 nm (Fig 9). Furthermore, we tried to synthesized larger iron oxide nanoparticles by varying the heating rates and higher temperature. In the case of varying the heating rates, there are no significant changes in size and shapes (Fig 8). in the case of the iron oxide nanoparticles synthesized at higher temperature (568 K), The size of the iron oxide nanoparticles is increased in TEM images but agglomeration occurred (Fig 9, 10).

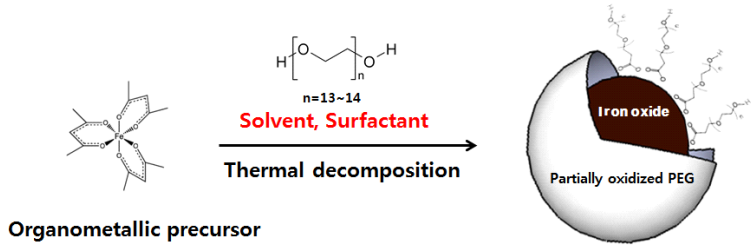

Scheme 1. Schematic illustration of iron oxide nanoparticles synthesis using organometallic precursor, ferric acetylacetonate

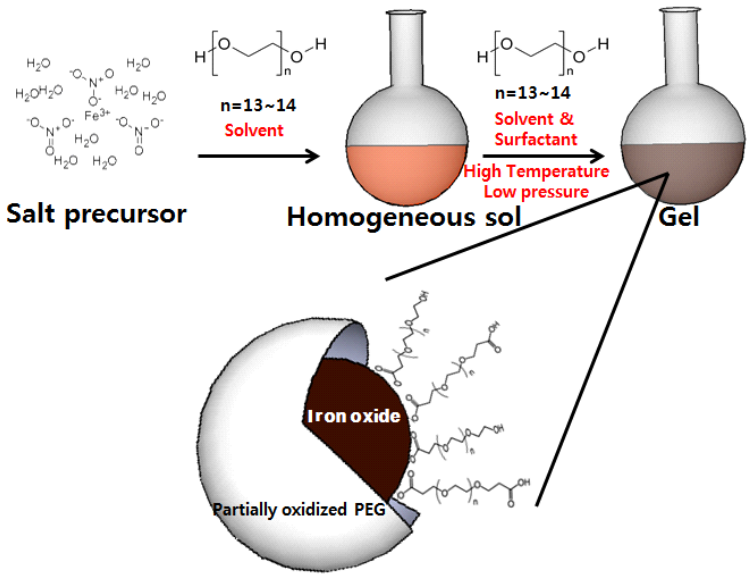

Scheme 2. Schematic illustration of iron oxide nanoparticles synthesis using salt precursor, ferric nitrate

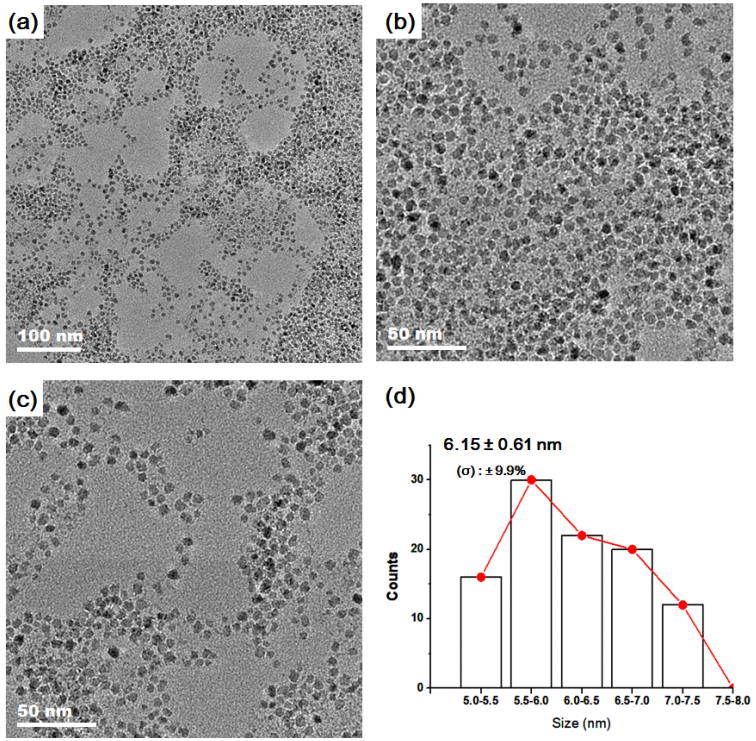

Fig 1. TEM images of the as-synthesized iron oxide nanoparticles with 0 h aging time at (a) low magnification, and (b, c) higher magnification, respectively. (d) Size distribution of iron oxide nanoparticles from randomly selected 100 pieces of TEM images.

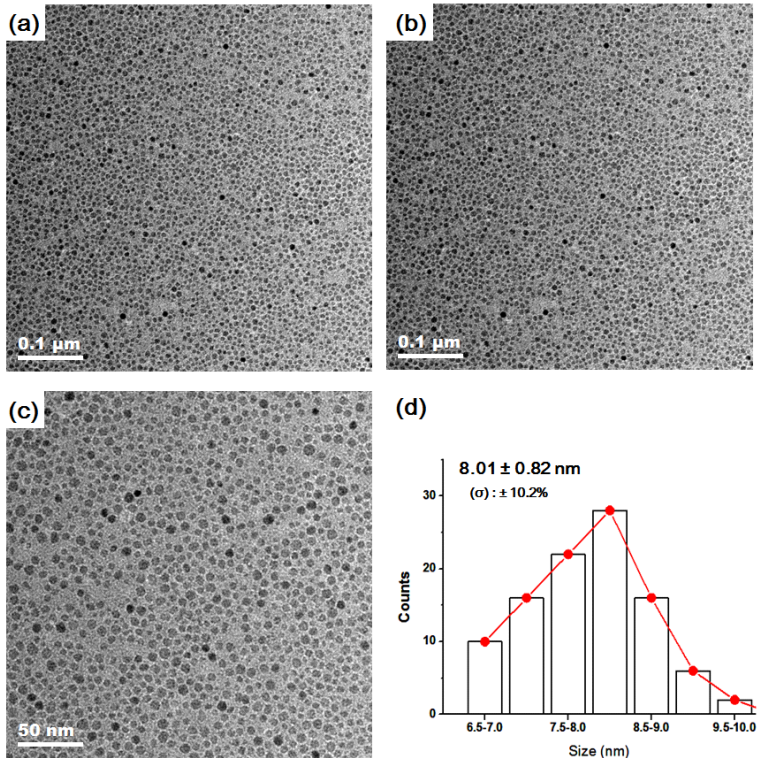

Fig 2. TEM images of the as-synthesized iron oxide nanoparticles with 0.5 h aging time at (a) low magnification, and (b, c) higher magnification, respectively. (d) Size distribution of iron oxide nanoparticles from randomly selected 100 pieces of TEM images.

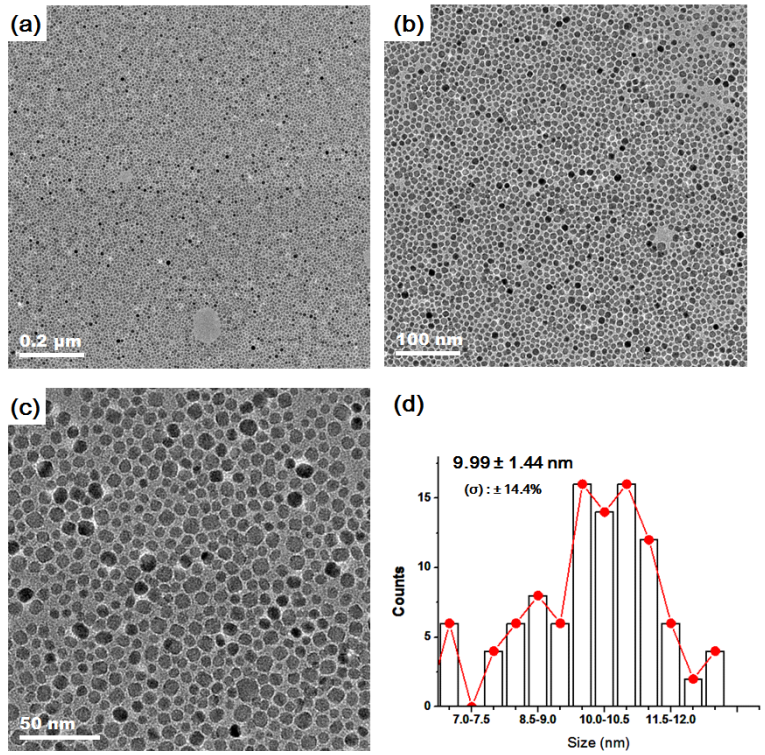

Fig 3. TEM images of the as-synthesized iron oxide nanoparticles with 1.5 h aging time. Image taken at (a) 20,000 × magnification, (b) 40,000 × magnification, and (c) 100,000 × magnification, respectively. (d) Size distribution of iron oxide nanoparticles from randomly selected 100 pieces of TEM images.

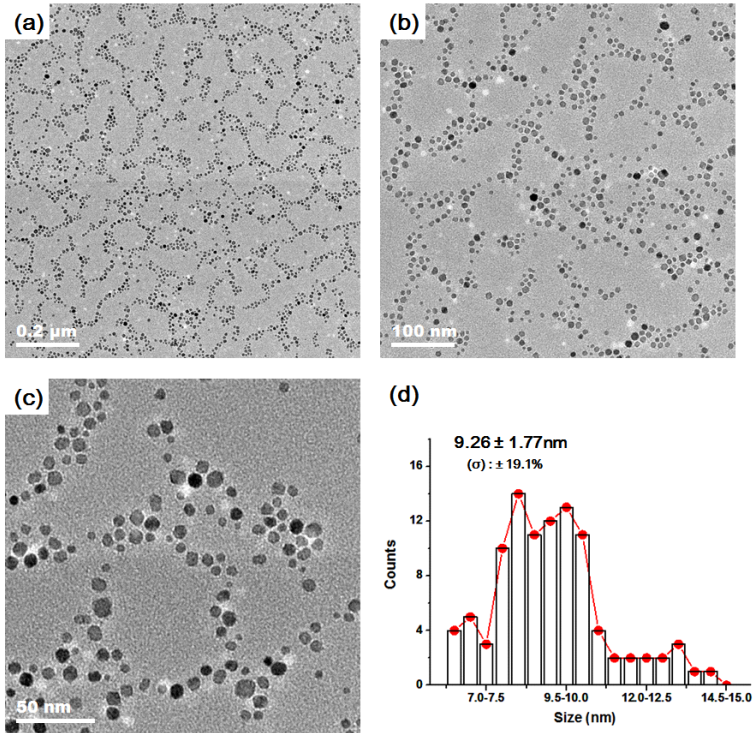

Fig 4. TEM images of as-synthesized iron oxide nanoparticles. Image taken at (a) 20,000 × magnification, (b) 40,000 × magnification, and (c) 100,000 × magnification, respectively.

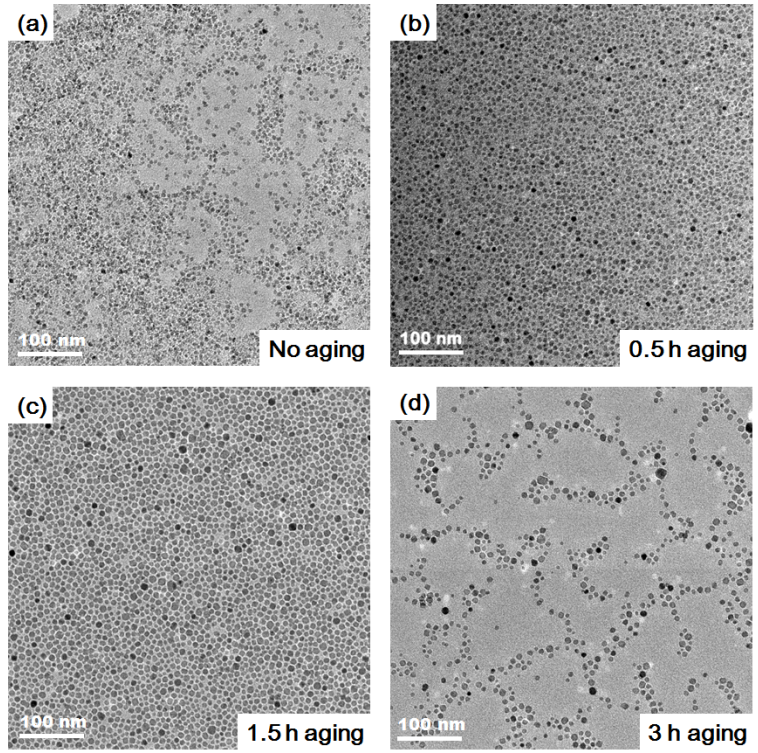

Fig 5. TEM images of the as-synthesized iron oxide nanoparticles with different aging times of (a) 0 h, (b) 0.5 h, (c) 1.5 h, and (d) 3 h, respectively. All images are taken at 40,000 × magnification.

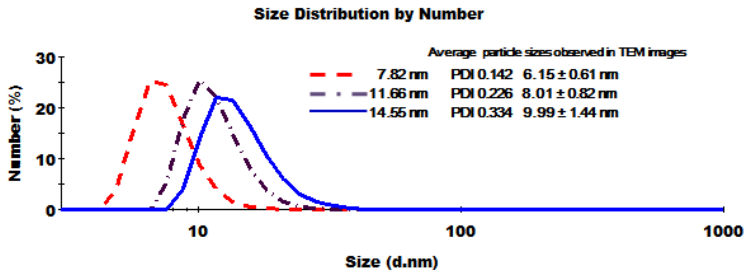

Fig 6. DLS data of the iron oxide nanoparticles prepared using ferric acetylacetonate with different aging times of no aging (dashed line, 6.15 ± 0.61 nm from TEM observations), 0.5 h aging (dashed dot line, 8.01 ± 0.82 nm from TEM observations), 1.5 h aging (solid line, 9.99 ± 1.44 nm from TEM observations) respectively.

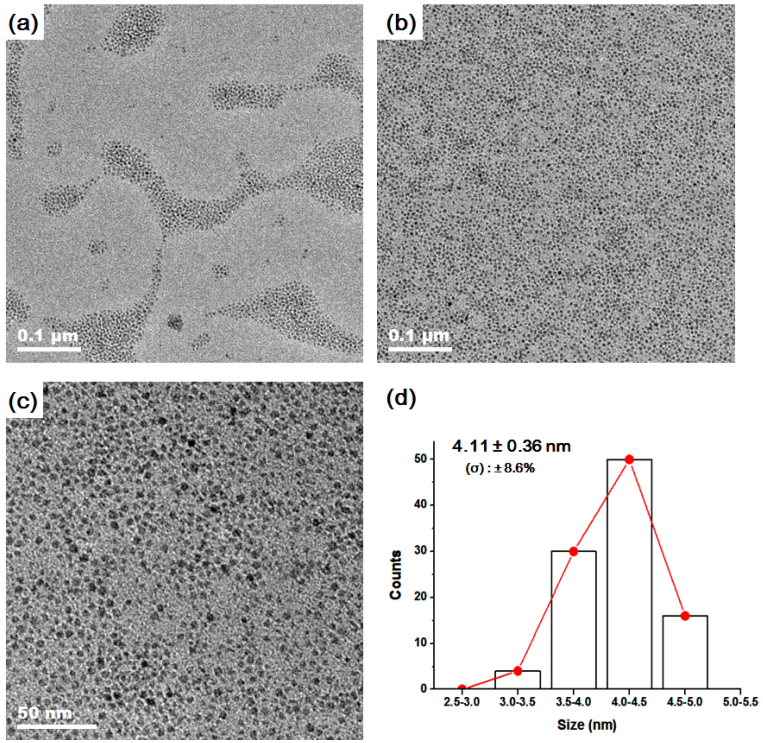

Fig 7. (a, b) low magnification and (c) relatively higher magnification TEM images of 4.11 ± 0.36 nm iron oxide nanoparticles prepared using ferric nitrate. (d) Size distribution of iron oxide nanoparticles from randomly selected 100 pieces of TEM images.

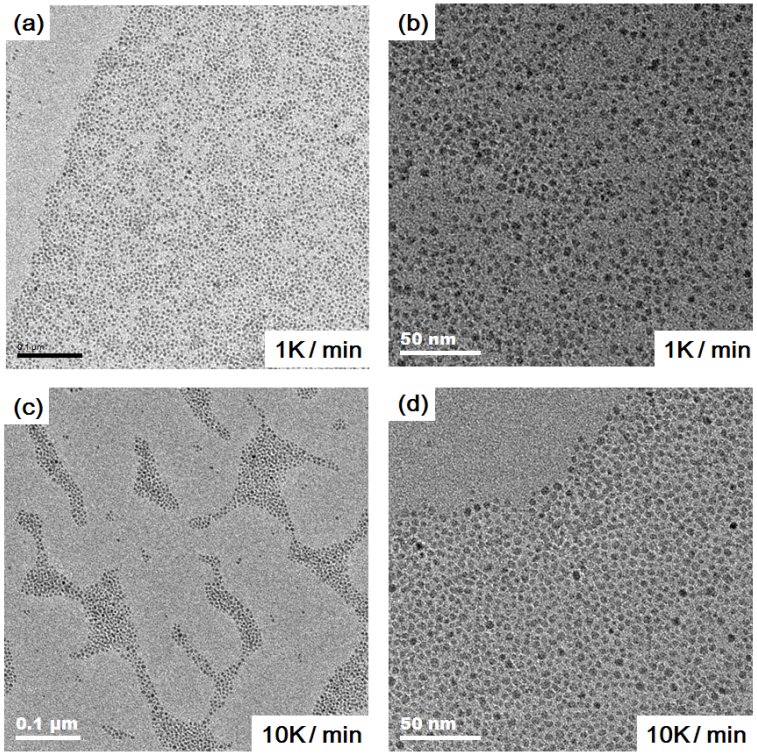

Fig 8. TEM images of the iron oxide nanoparticles using ferric nitrate with different heating rate of (a, b) 1K / min, and (c, d) 10 K / min. (The heating temperature for both samples is 538 K and maintain at that temperature for 30 min).

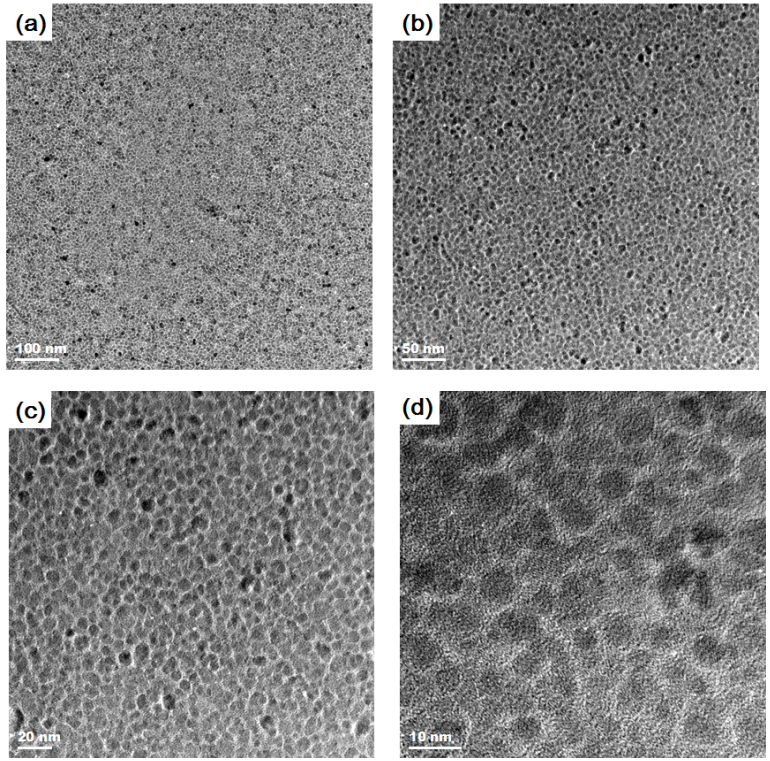

Fig 9. TEM images of the iron oxide nanoparticles synthesized at 568 K Image taken at (a) 20,000 × magnification, (b) 40,000 × magnification, (c) 100,000 × magnification, and (d) 300,000 × magnification, respectively.

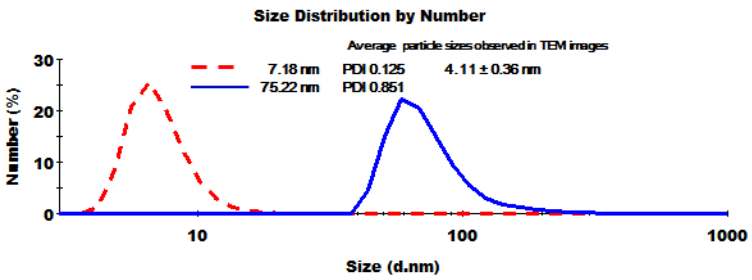

Fig 10. DLS data of the 4.11 ± 0.36 nm (from TEM observation) iron oxide nanoparticles using ferric nitrate (dashed line) and the aggregated iron oxide nanoparticles synthesized at 568 K (solid line).

3.3 XRD measurements of the as-synthesized iron oxide nanoparticles

The crystal structure of the as-synthesized iron oxide nanoparticles was confirmed by XRD analysis. Patterns of the as-synthesized iron oxide nanoparticles are summarized in (Fig 11 (A)), which were matched with (JCPDS # 00-019-0629). (200), (311), (400), (422), (511) and (440) peaks were associated with the inverse spinel structures of magnetite, although the (111) peak could not be distinguishable because of the overlap pattern of surface molecule, PEG [67]. Furthermore, XRD patterns of magnetite and maghemite is almost similar. Therefore, it is hard to distinguish between magnetite and maghemite with XRD measurement. Hence, we further studied the crystal structure of the iron oxide nanoparticles by using FT-IR analysis, will be described below. Furthermore, the XRD patterns of the as-synthesized iron oxide nanoparticles became narrow with the size increasing and peak of the (440) shown in (Fig 11 (B)). The crystalline size of the as-synthesized iron oxide nanoparticles were calculated by using Debye-Scherrer equation $t = K\lambda / \beta\cos\Theta$ where t is the crystalline size, λ is the x-ray wavelength, β is the (full width at half maximum) FWHM, Θ is the bragg's angle and K is the shape factor. In this study, we used the value K=0.9, λ=1.54 Å. The calculated crystalline sizes from (440) peak were matched with the observed TEM images (Table 3).

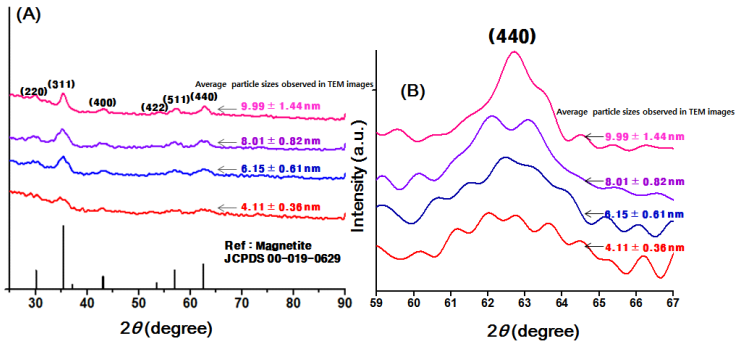

Fig 11. (a) XRD patterns of the as-synthesized iron oxide nanoparticles. 4.11 ± 0.36 nm (from TEM observation) iron oxide nanoparticles were synthesized using ferric nitrate as precursors. 6.15 ± 0.61 nm, 8.01 ± 0.82 nm, 9.99 ± 1.44 nm (from TEM observation) iron oxide nanoparticles were synthesized using ferric acetylacetonate. (b) XRD patterns of (440) peak of the iron oxide nanoparticles with different diameter.

Calculated crystalline size using Debye-scherrer equation at (440)	TEM images	DLS measurement
3.81 nm	4.11 ± 0.36 nm (σ) : ± 8.6 %	7.18 ± 0.89 nm PDI : 0.125
4.76 nm	6.15 ± 0.61 nm (σ) : ± 9.9 %	7.82 ± 1.11 nm PDI : 0.142
6.36 nm	8.01 ± 0.82 nm (σ) : ± 10.2 %	11.66 ± 2.64 nm PDI : 0.226
9.24 nm	9.99 ± 1.44 nm (σ) : ± 14.4 %	14.55 ± 4.86 nm PDI : 0.334

Table 3. The comparison of particle sizes by Debye-Scherrer equation, with the observed TEM images, and DLS measurements.

*(σ) : Standard deviation

*PDI : Polydispersity index

3.4 Surface study of the as-synthesized iron oxide nanoparticles

There are early study of the interaction between polymer and iron oxide nanoparticles. Li et al. reported that adsorption of the oleic acid on the surface of Fe_3O_4 nanoparticles [68]. Zhang et al reported the attachment of polymethacrylic acid to Fe3O4 nanoparticles via coordination linkages between the carboxyl groups and Fe [69].

To study the interaction between polymer (PEG) and iron oxide in our synthetic procedure, we conducted TGA and FT-IR study. TGA measurement of the as-synthesized iron oxide nanoparticles was carried out from 25 to 700 ℃ with a heating rate of 10℃ / min in air condition. Thermal degradation of the as-synthesized iron oxide nanoparticles are derived from the thermal degradation of the surface's organic molecules, which are densely covered iron oxide nanoparticles with 41.5 weight percentage (Fig 12). To investigate a better understanding the covered organic molecules, we conducted FT-IR study. FT-IR is an appropriate technique to establish the attachment of the polymer onto the surface of the as-synthesized iron oxide nanoparticles. In FT-IR study, we can confirm iron oxide surface covered by PEG molecules. FT-IR spectra of PEG and PEG coated iron oxide nanoparticles using ferric nitrate and ferric acetylacetonate are shown in (Fig 13 (A)). The peak associated with PEG, C-O-C stretching at 1100 cm^{-1}, hydroxyl group at 3410 cm^{-1} with broad ranges, sp^3 C - H symmetric stretching at 2864 cm^{-1} appear in the spectrum of both iron oxide nanoparticles. In

addition, the lattice adsorption band from the iron oxide nanoparticles is at 590 cm^{-1} shown in (Fig 13 (B)) indicate that the as-synthesized iron oxide nanoparticles are predominately Fe_3O_4 [70].

Furthermore, peaks were related with carbonyl group arose in the both spectrum of the as-synthesized iron oxide nanoparticles, but they have difference tendency depends on the precursor in 1500 cm^{-1} ~ 1800 cm^{-1} ranges as shown in Fig 14. In the case of iron oxide nanoparticles synthesized using ferric acetylacetonate, vibrational band of carbonyl groups is at around 1679 cm^{-1}, which can be assigned to the carbonyl group of oxidized PEG coordinating with Fe on the surface of the particles like in the present work [71] and the 1598 cm^{-1} and 1452 cm^{-1} peaks were observed which are ascribed to the asymmetric and symmetric stretching vibrations of the $-C=O-O^-$ group, respectively.

In the case of the as-synthesized iron oxide nanoparticles synthesized using ferric nitrate, different tendency was observed. The overlapped weak stretching mode of the $-C=O$ group was observed at 1713 cm^{-1}. Also, asymmetric and symmetric stretching vibrations of $-C=O-O^-$ group were observed at 1568 cm^{-1} and 1452 cm^{-1} respectively. Characteristic absorption bands at the wave number 1635 cm^{-1} correspond to deformation vibrations of C-OH band thus will contribute to the overlapping. The result suggests the presence of free carboxyl groups in the case of iron oxide nanoparticles using ferric nitrate. It can be assumed that the further oxidation of PEG 600 molecules occurred by intermediately formed nitric acid [72]

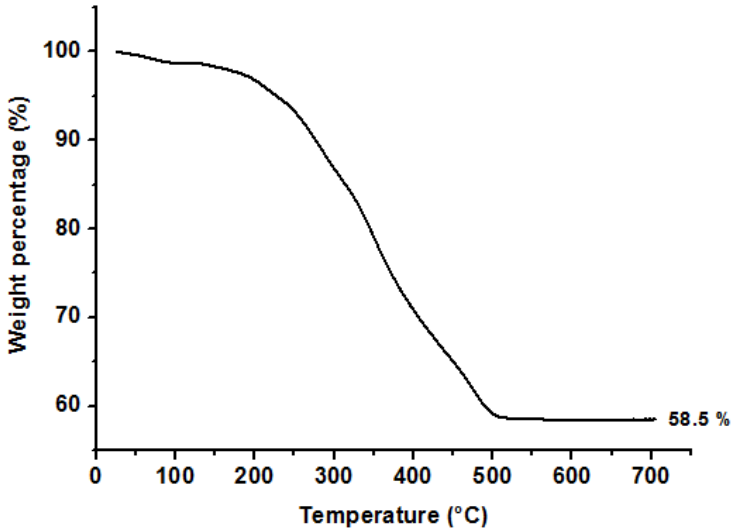

Fig 12. TGA data of the as-synthesized iron oxide nanoparticles (4.11 ± 0.36 nm from TEM observations) by using ferric nitrate

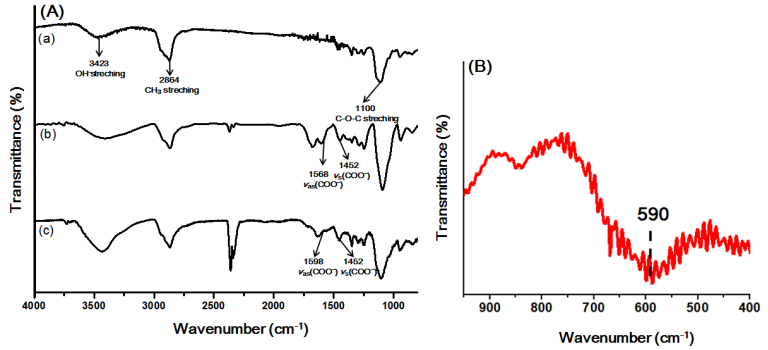

Fig 13. (a) is FT-IR spectrums of pure PEG 600 molecules. (b) FT-IR spectrum of the PEG coated iron oxide nanoparticles by using ferric acetylacetonate as precursor and, (c) by using ferric nitrate as precursor in (Fig 13 (A)). (Fig 13 (B)) show the lattice adsorption band spectrum of iron oxide nanoparticles by using ferric nitrate as precursor.

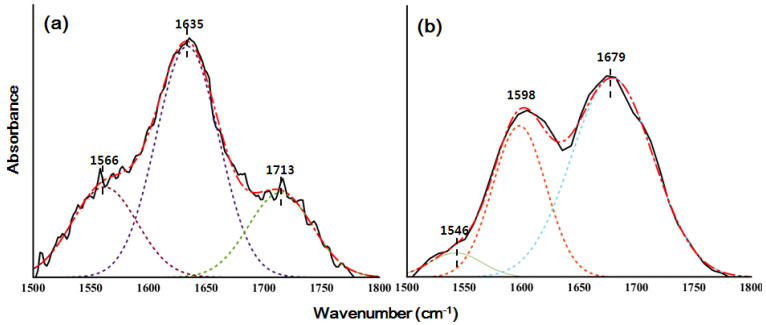

Fig 14. Gaussian fitted FT-IR spectrum of the as-synthesized iron oxide nanoparticles using ferric nitrate (a) and using ferric acetylacetonate (b) in 1500 cm^{-1} ~ 1800 cm^{-1} ranges. Fitted red dashed lines are calculated from the sum of the Gaussian peaks and black solid lines correspond to the original FT-IR spectrum.

3.5 Stability of the as-synthesized iron oxide nanoparticles

Stability of the nanoparticles is the most important property for biological and medical applications. Moreover, stability of the nanoparticles can be related to surface's molecules. Especially, PEG molecules are attracted much attention as surface molecules from there biocompatibility with colloidal stability enhancement properties due to steric repulsion of the PEG chains on the particle surface [73].

In this study, as-synthesized iron oxide nanoparticle's surfaces are covered by PEG molecules in synthetic procedure as we confirmed, so it could be expected a good colloidal stabilities. The colloidal stabilities of the as-synthesized iron oxide nanoparticles was investigated as a function of salt concentration and pH. The colloidal stabilities of the as-synthesized iron oxide nanoparticles in the presence of salt observed in 0.05 M to 0.75 M NaCl with 0.01 M PBS ph 7.4 solution. There are no precipitation or aggregation observed over 30 days (Fig 15 (a)). This high stabilities came from the PEG molecules, which are densely covered the iron oxide nanoparticle's surface.

The stability of the dispersed nanoparticles is strongly depends on the net surface charge that is also affected by the pH. The as-synthesized iron oxide nanoparticle's zeta potential and initial hydrodynamic size in 0.01 M PBS media at broad ranges of pH were plotted in Fig 16. The as-synthesized iron oxide nanoparticles have

an isoelectric point about pH 2.5 from the Zeta potential measurements. The iron oxide nanoparticles were well dispersed in broad ranges pH (from pH 3.3 to 12.2) solution over 1 month, while iron oxide nanoparticles dispersed in pH 2.5 solution were tend to aggregate and form a tubrid dispersion that is completely precipitated over 4 days as shown in Fig 15(b). In this result, we could observed the as-synthesized iron oxide nanoparticles are very stable over broad ranges pH and salt concentration because of their surface molecules, PEG.

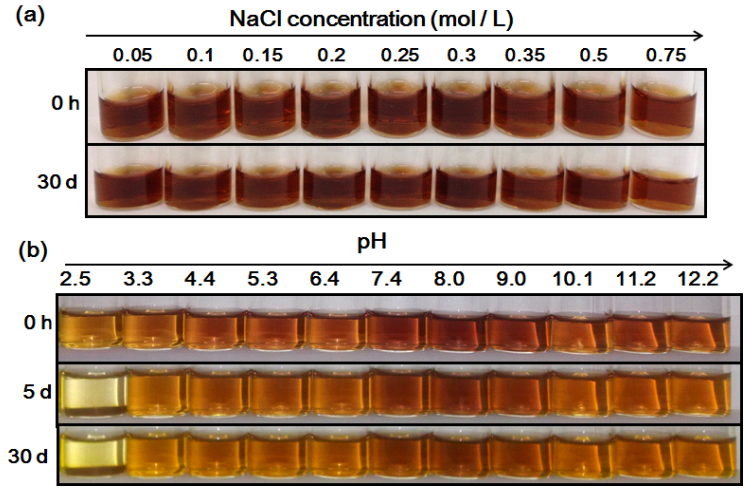

Fig 15. (a) Photograph of the as-synthesized iron oxide nanoparticles in various NaCl concetrations. (b) Photograph of the as-synthesized iron oxide nanoparticles in various pH conditions.

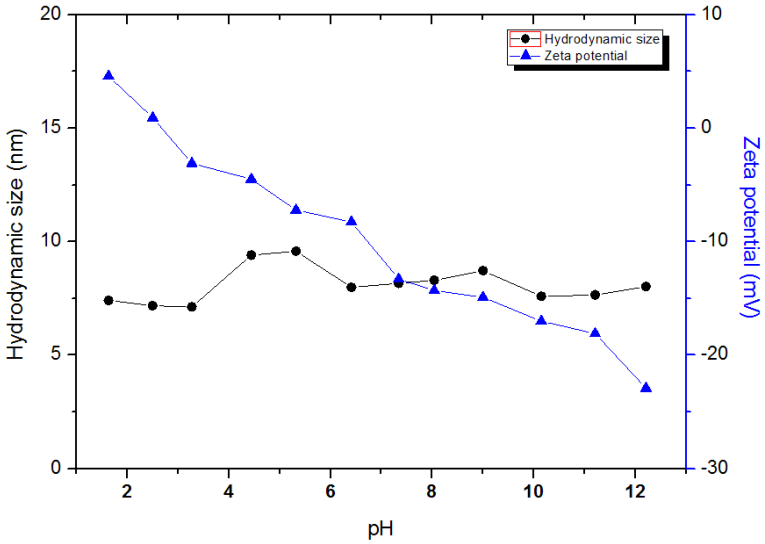

Fig 16. Zeta potential and Hydrodynamic sizes of the iron oxide nanoparticles in various pH conditions.

3.6 Surface functionalization of the as-synthesized iron oxide nanoparticles

The development of sensitive molecular imaging nanomaterials is very important for biomedical applications. Especially, multimodal imaging techniques based on the multimodal imaging agents have attracted much attention nowadays. In this work further functionalize for multimodal imaging, as-synthesized 4.11 ± 0.36 nm iron oxide nanoparticles by using the surface free carboxylic acid group of iron oxide nanoparticles. Functionalization steps were divided into two steps (Scheme 3 (A)). First, amine functionalization of the terminal carboxylic acid group was conducted via EDC / NHS coupling (Scheme 3 (B)). Second, RITC and NOTA were attatched to the iron oxide nanoparticle's surface via reaction of isothiocyatnate groups of the RITC / NOTA with surface's amine groups of the amine functionalized iron oxide nanoparticles (Scheme 3 (C)). The spectrums of RITC and NOTA molecules attached iron oxide nanoparticles are shown in (Fig 17). The fluorescent spectrum indicated that RITC molecules were attached to the iron oxide nanoparticles also DLS data show agglomeration not occurred during the functionalization of the iron oxide nanoparticles (Fig 18).

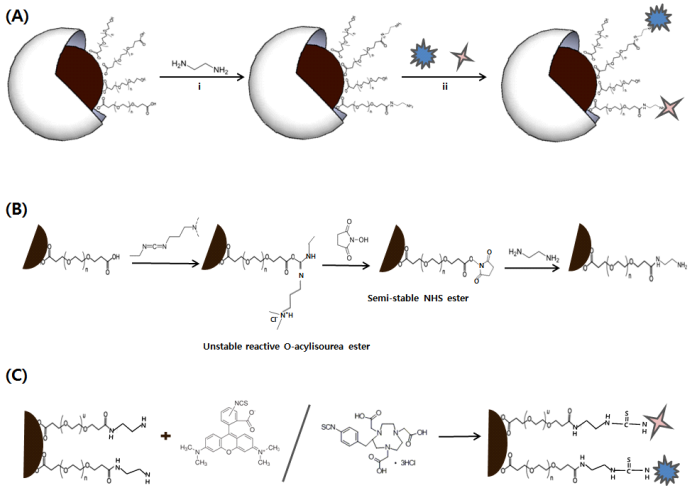

Rhodamine b isothiocyanate (RITC) as fluorescent dye

(2-(p-Isothiocyanatobenzyl)-1,4,7- triazacyclononane –N,N',N,"-triacetic acid trihydrochloride) ((p-SCN-Bn)-NOTA) as chelating agents of radioisotope

Scheme 3. Schematic illustration of the procedure for the functionalization

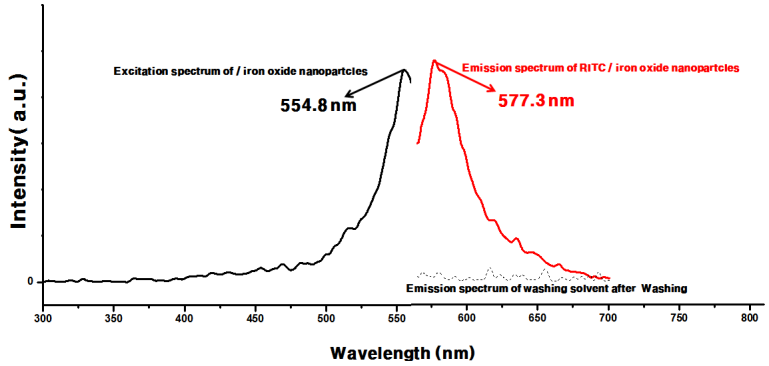

Fig 17. Excitation and emission spectra of RITC & NOTA conjugated iron oxide nanoparticles.

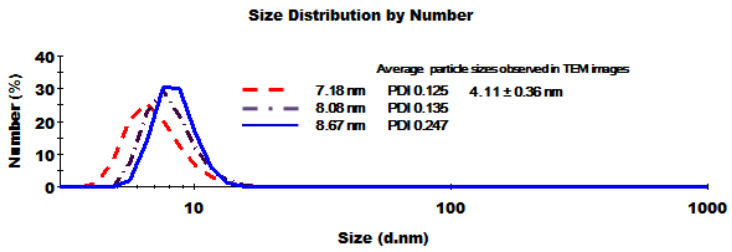

Fig 18. DLS data of the as-synthesized iron oxide nanoparticles (dashed line), RITC conjugated iron oxide nanoparticles (dashed dot line), RITC/NOTA conjugated iron oxide nanoparticles (solid line).

4. Conclusions

In this study, water well-dispersible iron oxide nanoparticles were synthesized in an one-pot reaction. The water-dispersible iron oxide nanoparticles were synthesized in the PEG 600 solution without additional surfactant, through simple polyol process by using two different types of precursor. In both cases, PEG 600 molecules was oxidized during the synthesis of the iron oxide nanoparticles. As a result, adsorption of partially oxidized PEG molecules to iron oxide nanoparticles is observed in both reactions even though there adsorption phenomena has slightly different tendency in FT-IR analysis. 6.15 ± 0.61 nm, 8.01 ± 0.82 nm, 9.99 ± 1.44 nm size of iron oxide nanoparticles were synthesized through the thermal decomposition of ferric acetyl acetonate as precursor in PEG 600 molecules by varying the aging times. The more smaller size (4.11 ± 0.36 nm from TEM observations) iron oxide nanoparticles were synthesized by using ferric nitrate as precursor.

Furthermore, the surface of the as-synthesized 4.11 ± 0.36 nm iron oxide nanoparticle was functionalized with the optical imaging agents and radioisotope chelating molecules to examine the possibility for multimodal imaging. Ethylenediamine was introduced to surface of iron oxide nanoparticles via EDC/NHS coupling. The resulting amine functionalized iron oxide nanoparticles were conjugated with RITC and NOTA through the reaction of isothiocyanate group with amine group at R.T. The conjugated reactions were confirmed by PL spectrum. The synthesized multifunctional iron oxide nanoparticles have a possibility to multimodal imaging agents.

References

[1] C. Buzea, I. I. Pacheco, K, Robbie, *Biointerphases.*, 2007, **2**, 17-71.

[2] V. S. Zaitsev, D. S. Filimonov, I. A. Presnyakov, R. J. Gambino, B. Chu, *J. Colloid Interface Sci.*, 1999, **212**, 49-57.

[3] M. A. El-sayed, *Acc. Chem. Res.*, 2001, **34**, 257-264.

[4] T. Takagahara, K. Takeda, *Phys. Rev. B.*, 1992, **46**, 578-581.

[5] R. Hao, R. Xing, Z. Xu, Y. Hou, S. Gao, S. Sun, *Adv. Mater.*, 2010, **22**, 2729-2742.

[6] J. W. M. Bulte, D. L. Kraitchman, *NMR biomed.*, 2004, **17**, 484-499.

[7] D. Artemov, N. Mori, B. Okollie, Z. M. Bhujwalla, *Magn. Reson. Med.*, 2003, **49**, 403-408.

[8] A. S. Arbab, L. A. Bashaw, B. R. Miller, E. K. jordan, B. K. Lewis, H. Kalish, J. A. Frank, *Radiology*, 2003, **229**, 838-846.

[9] J. Panyam, V. Labhasetwar, *Adv. Drug. Deliv. Rev.*, 2003, **55**, 329-347.

[10] K. S. Soppimath, T. M. Aminabhavi, A. R. Kulkarni, W. E. Rudzinski, *J. Controlled Release*, 2011, **70**, 1-20.

[11] S. A. Agnihotri, N. N. Mallikarjuna, T. M. Aminabhavi, *J. Controlled Release.*, 2004, **100**, 5-28.

[12] G. J. Wang, N. D. Volkow, P. K. Thanos, J. S. Fowler, *J. Addict. Dis.*, 2008, **23**, 39-53.

[13] J. Kim, Y. Piao, T. Hyeon, *Chem. Soc. Rev.*, 2009, **38**, 372-390.

[14] B. J. Pichler, M. S. Judenhofer, H. F. Wehrl, *Eur. Radiol.*, 2008, **18**, 1077-1086.

[15] H. P. W. Schlemmer, B. J. Pichler, M. Schmand, Z. Burbar, C. Michel, R. Ladebeck, K. Jattke, D. Townsend, C. Nahmias, P. K. Jacob, W. D. Heiss, C. D. Claussen, *Radiology*, 2008, **248**, 1028-103.

[16] W. A. D. Heer, P. Milani, A. Chatelain, *Phys. Rev. Lett.*, 1990, **65**, 488-491.

[17] M. Colombo, S. C. Romero, M. F. Casula, L. Gutierrez, M. P. Morales, I. B. Bohm, J. T. Heverhagen, D. Prosperi, W. J. Parak, *Chem. Soc. Rev.*, 2012, **41**, 4306-4334.

[18] R. H. Kodama, *J. Magn. Magn. Mater.*, 1999, **200**, 359-372.

[19] A. K. Gupta, M. Gupta, *Biomaterials*, 2005, **26**, 3995-4021.

[20] D. K. Kim, Y. Zhang, W. Voit, K. V. Rao, M. Muhammed, *J. Magn. Magn. Mater.*, 2001, **225**, 30-36.

[21] D. M. Cox, D. J. Trevor, R. L. Whetten, E. A. Rohlfing, A. Kaldor, *Phys. Rev. B.*, 1985, **32**, 7290-7298.

[22] C. Antoniak, J. Lindner, M. Farle, *Europhys. Lett.*, 2005, **70**, 250-256.

[23] Y. Piao, A. Burns, J. Kim, U. Wiesner, T. Hyeon, *Adv. Funct. Mat.*, 2008, **18**, 3745-3758.

[24] T. Neuberger, B. Schopf, H. Hofmann, M. Hofmann, B. V.

Rechenberg, *J. Magn. Magn. Mater.*, 2005, **293**, 483-496.

[25] L. Babes, B. Denizot, G. Tanguy, J. J. L. Jeune, P. Jallet, *J. Colloid Interface Sci.* 1999, **212**, 474-482.

[26] L. A. Welo, O. Baudisch, *Philos. Mag.*, 1925, **50**, 399-408.

[27] A. B. Bourlinos, A. Bakandritsos, V. Georgakilas, D. Petridis, *Chem. Mater.*, 2002, **14**, 3226-3228.

[28] N. Bao, L. Shen, Y. Wang, P. Padhan, A. Gupta, *J. Am. Chem. Soc.*, 2007, **129**, 12374-12375.

[29] S. Santra, R. Tapec, N. Theodoropoulou, J. Dobson, A. Hebard, W. Tan, *Langmuir*, 2001, **17**, 2900-2906.

[30] G. Ennas, A. Musinu, G. Piccaluga, D. Zedda, *Chem. Mater.*, 1998, **10**, 495-502.

[31] M. Niederberger, *Acc. Chem. Res.*, 2007, **40**, 793-800.

[32] M. Niederberger, G. Garnweitner, N. Pinna, G. Neri, *Prog. Solid State Chem.*, 2005, **33**, 59-70.

[33] W. W. Yu, J. C. Falkner, C. T. Yavuz, V. L. Colvin, *Chem. Commun.*, 2004, 2306-2307.

[34] M. M. Titirici, M. Antonietti, A. Thomas, *Chem. Mater.*, 2006, **18**, 3808-3812.

[35] S. Sun, H. Zeng, *J. Am. Chem. Soc.*, 2002, **124**, 8204-8205.

[36] J. Park, K. An, Y. Hwang, J. G. Park, H. J. Noh, J. Y. Kim, J. H. Park, N. M. Hwang, T. Hyeon, *Nat. Mater.*, 2004, **3**, 891-895.

[37] N. R. Jana, Y. Chen, X. Peng, *Chem. Mater.*, 2004, **16**, 3931-3935.

[38] H. B. Na, I. S. Lee, H. Seo, Y. I. Park, J. H. Lee, S. W. Kim, T. Hyeon, *Chem. Commun.*, 2007, 5167-5169.

[39] R. Hong, N. O. Fischer, T. Emrick, V. M. Rotello, *Chem. Mater.*, 2005. **17**. 4617-4621.

[40] N. J. J. Johnson, N. M. Sangeetha, J. C. Boyer, F. C. J. M. van Veggel, *Nanoscale*, 2010, **2**, 771-777.

[41] R. D. Palma, S. Peeters, M. J. V. Bael, H. V. den Rul, K. Bonroy, W. Laureyn, J. Mullens, G. Borghs, G. Maes, *Chem. Mater.* 2007, **19**, 1821-1831.

[42] J. Xie, C. Xu, N. Kohler, Y. Hou, S. Sun, *Adv. Mater.*, 2007, **19**, 3163-3166.

[43] F. M. Veronese, G. Pasut, *Drug. Discov. Today.*, 2005, **10**, 1451-1458.

[44] J. H. Lee, H. B. Lee, J. D. Andrade, *Prog. Polym. Sci.*, 1995, **20**, 1043-1079.

[45] D. Liu, W. Wu, J. Ling, S. Wen, N. Gu, X. Zhang, *Adv. Funct. Mater.*, 2011, **21**, 1498 - 1504.

[46] J. F. Lutz, S. Stiller, A. Hoth, L. Kaufner, U. Pison, R. Cartier, *Biomacromolecules*, 2006, **7**, 3132-3138.

[47] H. B. Na, G. Palui, J. T. Rosenberg, X. Ji, S. C. Grant, H. Mattoussi, *ACS Nano.*, 2012, **6**, 389-399.

[48] R. H. Concalves, Claudio. A. Cardoso, E. R. Leite, *J. Mater. Chem.*, 2010, **20**, 1167-1172.

[49] P. Calandra, M. Goffredi, V. T. Liveri, Collodis and Surfaces A 1999, **160**, 9-13.

[50] X. Zhao, R. P. Bagwe, W. Tan, *Adv. Mater.*, 2004, **16**, 173-176.

[51] X. Zhang, K. Y. Chan, *Chem. Mater.* **2003,** *15,* 451-459.

[52] J. V. Vidal, J. Rivas, M. A. L. Quintela, *Colloids. Surface. A.* 2006, **288**, 44-51.

[53] T. J. Daou, G. Pourroy, S. B. Colin, J. M Greneche, C. U. Bouillet, P. Legare, P. Bernhardt, C. Leuvrey, G. Rogez, *Chem. Mater.*, 2006, **18**, 4399-4404.

[54] S. Jeon, P. V. Braun, *Chem. Mater.*, 2003, **15**, 1256-1263.

[55] D. H. Chen, X. R. He, *Mater. Res. Bull.*, 2001, **36**, 1369-1377.

[56] J. Jia, B. Wang, A. Wu, G. Cheng, Z. Li, S. Dong, *Anal. Chem.*, 2002, **74**, 2217-2223.

[57] M. Niederberger, M. H. Bartl, G. D. Stucky, *J. Am. Chem. Soc.* 2002, **124**, 13642-13643.

[58] J. Ba, J. Polleux, M. Antonietti, M. Niederberger, *Adv. Mater.*, 2005, **17**, 2509 - 2512.

[59] Y. Ye, F. Yuan, S. Li, *Mater. Lett.*, 2006, **60**, 3175-3178.

[60] M. Niederberger, G. Garnweitner, *Chem. Eur. J.*, 2006, **12**, 7282 - 7302.

[61] I. Djerdj, G. Garnweitner, D. S. Su, M. Niederberger, *J. Solid. State. Chem.*, 2007, **180**, 2154-2165.

[62] T. Hyeon, S. S. Lee, J. Park, Y. Chung, H. B. Na, *J. Am. Chem. Soc.*, 2001, **123**, 12798-12801.

[63] S. G. Kwon, T. Hyeon, *Small*, 2011, **19**, 2685-2702.

[64] M. Niederberger, N. Pinna, *Metal Oxide Nanoparticles in Organic Solvents : Synthesis, Formation, Assembly and Application*, Springer, London, 2009.

[65] K. Wieczorek-Ciurowa, A. J. Kozak, *J. Therm. Anal. Calorim.*, 1999, **58**, 647-651.

[66] J. Xu, H. Yang, W. Fu, K. Du, Y. Sui, J. Chen, Y. Zeng, M. Li, G. Zou, *J. Magn. Magn. Mater.*, 2007, **309**, 307-311.

[67] J. Lheritier, A. Chauvet, J. Masse, *Thermochim. Acta.*, 1994, **241**, 157-169.

[68] P. Li, B. Yu, X. Wei, *J. Appl. Polym. Sci.*, 2004, **93**, 894-900.

[69] H. Zhang, R. Wang, G. Zhang, B. Yang, *J. Appl. Polym. Sci.*, 2003, **429**, 167-173.

[70] T. J. Daou, J. M. Greneche, G. Pourroy, S. Buathong, A. Derory, C. Ulhaq-Bouillet, B. Donnio, D. Guillon, S. Begin-Colin, *Chem. mater.*, 2008, **20**, 5869-5875.

[71] F. Hu, Q. Jia, Y. Li, M. Gao, *Nanotechnology*, 2011, **22**, 1-7.

[72] S. N. Rishikeshi, S. S. Joshi, M. K. Temgire, J. R. Bellare, *Dalton Trans.*, 2012, Article in press.

[73] B. Dubertret, P. Skourides, D. J. Norris, V. Noireaux, A. H. Brivanlou, A. Libchaber, *Science*, 2002, **298**, 1759-1762.

요 약 (국문초록)

본 연구에서는 다기능성을 갖는 산화철 나노입자의 합성을 시도하였다. 산화철 나노입자의 합성은 독성이 없는 Polyethylene glycol (PEG, MW=600)을 용매 및 capping agent로 이용하는 간단한 polyol process를 통해 합성하였으며 그 결과, 물에 안정적으로 분산되는 산화철 나노입자가 합성되었다. 나노 입자의 크기는 반응 시간 변화에 의해 제어되었다.

합성과정 중 PEG의 말단 수산기는 부분적으로 산화되어 카르복실 산으로 변환되었으며, 이를 통해 산화철 나노입자의 capping agent역할을 하게 된다. 산화철 나노 입자 표면에 코팅된 PEG 층은 푸리에 변환 적외선 분광 (FT-IR) 분석을 통하여 분석하였다.

합성된 산화철 나노입자는 투과 전자 현미경 (TEM) 및 동적 광 산란법 (DLS) 을 이용하여 분석하였다. TEM 을 통해 확인한 4.11 ± 0.36 nm 의 크기를 갖는 산화철 나노입자는 X선 회절 분석 (XRD) 패턴에서 Scherrer 방정식을 이용하여 계산된 3.81 nm 결정 크기와 유사한 크기를 갖는 것을 확인하였으며, 물에서의 유체 크기는 DLS를 이용하여 7.18 ± 0.89 nm 로 측정되었다. 또한 합성된 산화철 나노 입자가 폭 넓은 산도 범위 및 전해질 수용액에서도 매우 안정적임을 확인 하였다.

다기능 나노 입자로서의 가능성을 확인하기 위해 합성된 산화철 나노입자 표면 기능화를 시도하였다. 합성된 산화철 나노 입자는 일반적인 EDC / NHS 커플링 반응을 이용하여 아민 그룹을 도입하였다. 그리고 Rhodamine b isothiocyanate (RITC) 및 2-(ρ-Isothiocyanatobenzyl)-1,4,7-triazacyclononane - N,N′,N,″-triacetic acid trihydrochloride) ((ρ-SCN-Bn)-NOTA) 분자의 아이소싸이오사이아네이트기와 나노입자표면의 아민 그룹 반응을 이용하여 티오우레아 결합을 형성시킴으로서, 산화철 나노입자에 표면에 결합하였다. 산화철 나노입자에 결합된 RITC 분자는 Photoluminescence spectroscopy (PL) 스펙트럼을 통하여 산화철 표면에 잘 결합되었음을 확인하였다.

이렇게 합성된 물에 잘 분산되는 다기능의 산화철 나노입자는 수계에서의 안정성과 함께 다기능성을 갖고 있기 때문에 biological multimodal imaging에 이용 될 수 있을 것으로 기대된다.

주요어 : 산화철 나노입자, PEGylation, Polyol 합성, 다기능 나노입자

학 번 : 2011-22756